

Structural anisotropy in amorphous SnO₂ film probed by X-ray absorption spectroscopy

Q. Zhu,¹ Q. Ma,^{1,2,a)} D. B. Buchholz,¹ R. P. H. Chang,¹ M. J. Bedzyk,¹ and T. O. Mason¹

¹Department of Materials Science and Engineering, Northwestern University, Evanston, Illinois 60208, USA

²DND-CAT, Northwestern Synchrotron Research Center at Advanced Photon Source, Argonne, Illinois 60439, USA

(Received 12 April 2013; accepted 28 June 2013; published online 17 July 2013)

Polarization-dependent X-ray absorption measurements reveal the existence of structural anisotropy in amorphous (*a*-) SnO₂ film. The anisotropy is readily seen for the second neighbor interaction whose magnitude differs along three measured directions. The differences can be well accounted for by 10%–20% variation in the Debye-Waller factor. Instead of a single Gaussian distribution found in crystalline SnO₂, the Sn-O bond distribution is bimodal in *a*-SnO₂ whose separation shows a weak angular dependence. The oxygen vacancies, existing in the *a*-SnO₂ film in the order of 10²¹ cm⁻³, distribute preferentially along the film surface direction. © 2013 AIP Publishing LLC. [<http://dx.doi.org/10.1063/1.4815984>]

Transparent conducting oxides (TCOs), combining good electrical and optical properties, have been extensively used in technological applications such as photovoltaics and flat panel displays.¹ Amorphous TCOs, with comparable electrical and optical properties to their crystalline counterparts, are becoming promising alternatives, since they have better surface morphologies and no grain boundary or multiple grain orientations and can be deposited at lower temperatures and on flexible substrates.² However, the structures of amorphous TCOs are much less explored versus their crystalline counterparts.

It is well established that the structures of amorphous materials have the short-range order, as traditionally defined by the first and second well-separated peaks in their pair-distribution functions involving the bond length and bond angle.³ It is also a commonly held belief that these structures are isotropic due to the randomness.⁴ Therefore, the scope of the so-called order in amorphous states is narrow in the sense that anisotropy, one of the characteristics often associated with ordering as found in crystalline materials, is seldom recognized.⁵ Here we present a structural study of a conductive amorphous (*a*-) SnO₂ film using polarization-dependent X-ray absorption spectroscopy. Detailed analyses of the extended X-ray absorption fine structure (EXAFS) reveal the existence of structural anisotropy in this amorphous film and some significant departures from crystalline (*c*-) SnO₂, contrary to the report by Tafto *et al.*⁶

The *a*-SnO₂ thin film was deposited onto a 1 × 1 cm² glass substrate at room temperature by a pulsed laser deposition (PLD) system with a 248 nm KrF excimer laser. At nominal pO₂ pressure of 10 mTorr, the ~190-nm-thick film had conductivity, mobility, and carrier concentration of 535 S/cm, 17 cm²/V s, and 1.9 × 10²⁰/cm³, respectively. This deposition condition represents the onset for optimal transparent conductor behavior, as illustrated by the pO₂ dependence of deposition of a series of the slightly thicker films (see Figs. S1 and S2 in Ref. 7). Grazing incidence X-ray diffraction measurement

(Rigaku ATX-G Workstation, Tokyo, Japan) confirmed the lack of long-range order in this film (see Fig. S3 in Ref. 7).

X-ray absorption measurements were carried out at the 5BMD beamline of the DuPont-Northwestern-Dow-Collaborative Access Team (DND-CAT) at the Advanced Photon Source (Argonne, IL). Fig. 1 shows the schematic experimental setup. The synchrotron X-ray beam is linearly polarized in the direction perpendicular to its propagation direction in the horizontal plane. The sample was mounted so that its surface normal was in the horizontal plane with the polarization direction. Polarization-dependent X-ray absorption measurements were realized by rotating the sample around the axis perpendicular to both the surface normal and the X-ray beam directions. Measurements were carried out at $\theta = 12^\circ$, 52° , and 90° , respectively, in fluorescence mode at the Sn K edge using a 4-element Si drift detector (SII NanoTechnology). At $\theta = 90^\circ$, the detector is positioned such that the minimum take-off angle of detected Sn K_α fluorescence photons (~25 keV) is $>0.1^\circ$, the angle at which the fluorescence photons travel one absorption length in the 190-nm thick film. Therefore, its entire thickness is sampled as well. A double Si (111) crystal monochromator was used for energy selection with $\Delta E/E = 1.4 \times 10^{-4}$. The incident X-ray intensity was detuned by 60% of its maximum for harmonic rejection.

Commercial SnO₂ powder (99.99%, Aldrich) was used as the reference material. The powder was spread uniformly on a long Scotch tape (3M Corp.), which was then folded, and the absorption jump step is 0.5. X-ray absorption measurement was carried out in transmission mode using the ionization chambers (Oxford Danfysik). *c*-SnO₂ has a rutile structure⁸ (*Space group*: p42/mnm), in which Sn is surrounded by six O with two at 2.0457 Å and four at 2.0606 Å ($\Delta R = 0.0149$ Å). There are two Sn at a distance of 3.1900 Å.

Fig. 2(a) shows the k^3 -weighted EXAFS functions $\chi(k)$ vs. wave number k , extracted from the raw absorption data for *a*-SnO₂ and for powder *c*-SnO₂. The EXAFS spectra of *a*-SnO₂ show sinusoidal oscillations due to the disorder in amorphous films. Some weak differences are seen among the

^{a)} Author to whom correspondence should be addressed. Electronic mail: q-ma@northwestern.edu

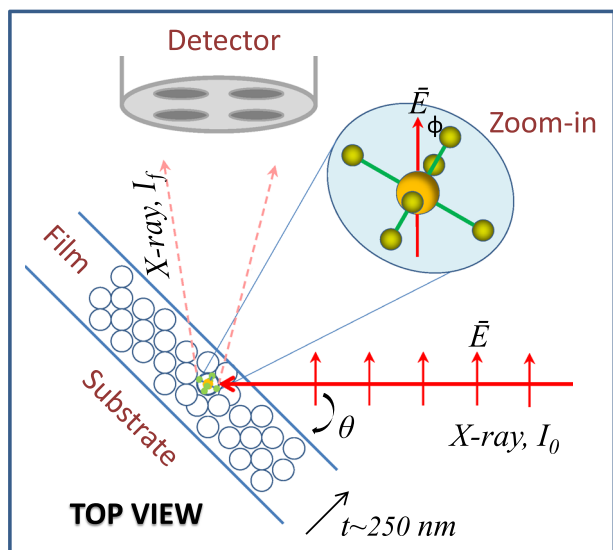


FIG. 1. Schematic top view of the experimental setup.

a-SnO₂ data measured at different angles. Fig. 2(b) shows the phase-uncorrected Fourier transforms (FT) of $k^3\chi(k)$ obtained using the data from $k=2.4$ to 12.4 \AA^{-1} applied with a Hanning window ($\Delta k=2 \text{ \AA}^{-1}$). The differences are clearly seen in the second peaks, being strongest along the film surface direction and weakest for $\theta=52^\circ$ which is close to the so-called magic angle 54.7° where the average structure should be measured.⁹ This suggests readily the existence of anisotropy in this *a*-SnO₂ film. The difference in the first peak exists but apparently weaker. With respect to the main peaks, the satellite peaks near $R=1 \text{ \AA}$ are considerably larger in *a*-SnO₂ than in *c*-SnO₂. Disorder can cause a similar effect, which is not the main cause here.

It is well known that $\chi(k)$ may be parameterized as¹⁰

$$\chi(k) = S_0^2 \sum_i \frac{N_i(\phi) |f_i(k)|}{kR_i^2} \sin[2R_i k + \phi_i(k)] e^{-2\sigma_i^2 k^2}. \quad (1)$$

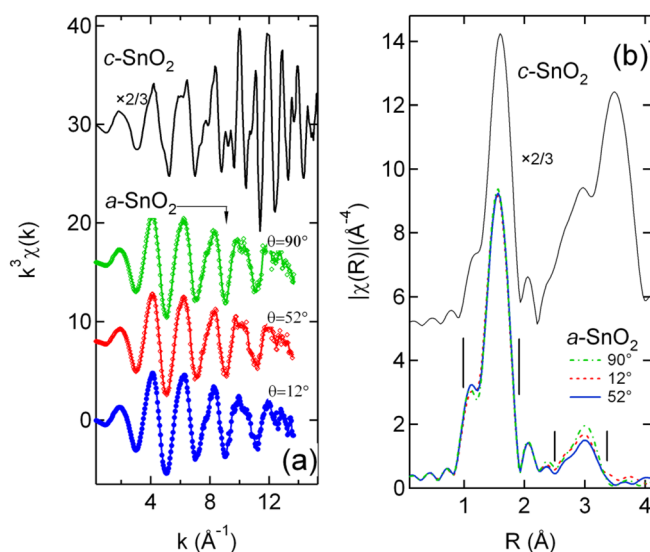


FIG. 2. (a) The k^3 -weighted EXAFS spectra of *a*-SnO₂ measured at three X-ray incident angles. Circles: raw data. Solid lines: smoothed data. Also shown is the EXAFS data of *c*-SnO₂. (b) Fourier transforms of $k^3\chi(k)$, using the data from $k=2.4$ to 12.4 \AA^{-1} and a Hanning window with $\Delta k=2$. The vertical lines define the first and second peak regions. A reduction factor of 2/3 is applied to the *c*-SnO₂ data.

In Eq. (1), only harmonic oscillators are assumed, since the high-order cumulant effect (>2) is negligible for *c*-SnO₂, which seems to be the case for *a*-SnO₂ as well. The photoelectron mean free path effect ($e^{-2R_i/\lambda(k)}$) is also omitted. It is thus assumed that $\lambda(k)$ is identical for *c*-SnO₂ and *a*-SnO₂. To determine the bond distance R_i and coordination number N_i , prior knowledge of $\phi(k)$, S_0^2 , and $f_i(k)$ are needed. S_0^2 , the passive loss of the photoelectron, is primarily related to the absorbing atom. It can be safely extracted from a known structure, i.e., *c*-SnO₂ in this case. $\phi_i(k)$ is the phase shift due to the scattering of the photoelectron. $f_i(k)$ is the backscattering amplitude of neighboring atoms. Both $\phi_i(k)$ and $f_i(k)$ are generated from the FEFF calculation using the *c*-SnO₂ structure. $e^{-2\sigma_i^2 k^2}$ is the Debye-Waller factor where σ^2 is the root mean square of the bond distance fluctuation about the arithmetic mean, a measure of its disorder. For a disordered system, $N(\phi) (= \sum_i^N 3 \cos^2 \phi_i)$ may not be expected, where ϕ is the angle between the X-ray polarization direction and a chemical bond (see Fig. 1). Note that N_i is fixed during the fittings while S_0^2 is varied. Changes seen in S_0^2 translate ultimately into N_i since $S_0^2 = \text{constant}$. The data processing is carried out using the Athena and Artemis software package.¹¹

The prevailing knowledge about the local structures of amorphous phases is that they are similar to their crystalline counterparts, in terms of bond lengths and coordination numbers. Fitting the first peak with a single Sn-O bond length and $N=6$ shows that $R=2.051 \pm 0.003 \text{ \AA}$ and $\sigma^2=0.0060 \pm 0.0003 \text{ \AA}^2$ for *a*-SnO₂. However, the S_0^2 value shows a k_{max} -dependence, as displayed in Fig. 3. k_{max} is the upper bound of $\chi(k)$ used in the fitting. For the fittings using the data with $k_{\text{max}} > 11.0 \text{ \AA}^{-1}$ the figure of merit (not shown here) deteriorates by 3-to-5 fold due in part to the increased

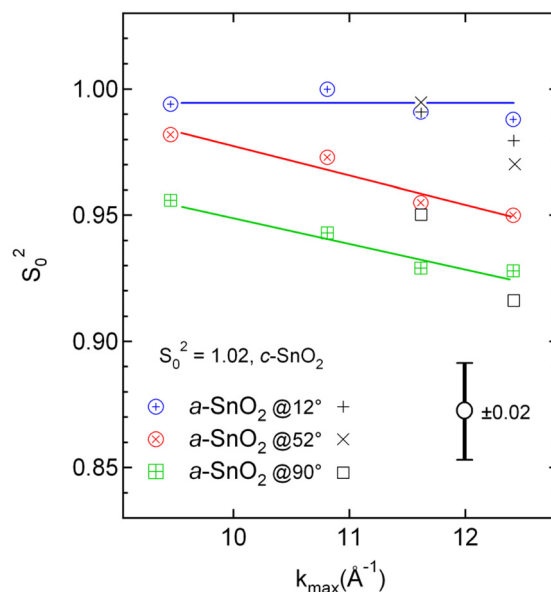


FIG. 3. k_{max} -dependence of S_0^2 for the *a*-SnO₂ film measured at $\theta=12^\circ$, 52° , and 90° , respectively. The fitting results obtained with assuming a single Sn-O distance and $N=6$ are shown by the circle/+ symbols at 12° , the circle/ \times symbols at 52° , and the square/+ symbols at 90° . The results obtained assuming two Sn-O distances and $N_1+N_2=6$ are shown by + at 12° , \times at 52° , and \square at 90° . Lines are to guide the eyes only. S_0^2 for *c*-SnO₂ is determined using the data up to 14.7 \AA^{-1} where the first shell EXAFS oscillations are essentially complete.

magnitude of the satellite peak. This is in fact due likely to the existence of more than one Sn-O bond distance in the first shell. It can be shown that S_0^2 decreases in the case of a small separation of two identical bonds, since it is inversely proportional to a $\cos(2k\Delta R)$ -containing term.¹² Their interference affects dominantly high k range. The S_0^2 value may drop 10% from $k_{max} = 10$ to 12 \AA^{-1} due to the $\cos(2k\Delta R)$ term alone for $\Delta R = 0.1 \text{ \AA}$. For a short data range such as $k_{max} = 9.5 \text{ \AA}^{-1}$, the effect can be approximated by $e^{-2\Delta\sigma^2 k^2}$. More discussion can be found in Ref. 7 (see Figs. S4 and S5). Note that for $c\text{-SnO}_2$, S_0^2 is obtained using with $k_{max} = 14.7 \text{ \AA}^{-1}$, $R = 2.0548 \text{ \AA}$, and $\sigma^2 = 0.0028 \text{ \AA}^2$.

Fig. 4 displays the fitting results under various conditions. As shown, a single Sn-O bond distance describes nearly perfectly the first shell EXAFS of $c\text{-SnO}_2$. However, the fitting qualities are inferior for $a\text{-SnO}_2$ under this conditions, and large discrepancies in the phases are seen; the discrepancy is smaller for $12^\circ\text{-}\chi(k)$. Assuming two Sn-O bond distances and $N_1 + N_2 = 6$, the fitting qualities are improved remarkably. As presented in Fig. 3, the k_{max} -dependence of S_0^2 is largely removed. It is however less so for $90^\circ\text{-}\chi(k)$ at $k_{max} = 12.4 \text{ \AA}^{-1}$, which may be affected adversely by the noise near the data end; the effect may exist for $12^\circ\text{-}\chi(k)$ and $52^\circ\text{-}\chi(k)$ as well. Instead of a single Gaussian-like distribution of the Sn-O bond in $c\text{-SnO}_2$, the Sn-O bond distribution appears to be bimodal in $a\text{-SnO}_2$. Note that the θ -dependence of S_0^2 (or N) seems to persist and is preserved roughly to the findings obtained using the short range data. A significant decrease in S_0^2 is seen, i.e., a large reduction in N from 5.9 for $\theta = 12^\circ$ to 5.6 for $\theta = 90^\circ$.

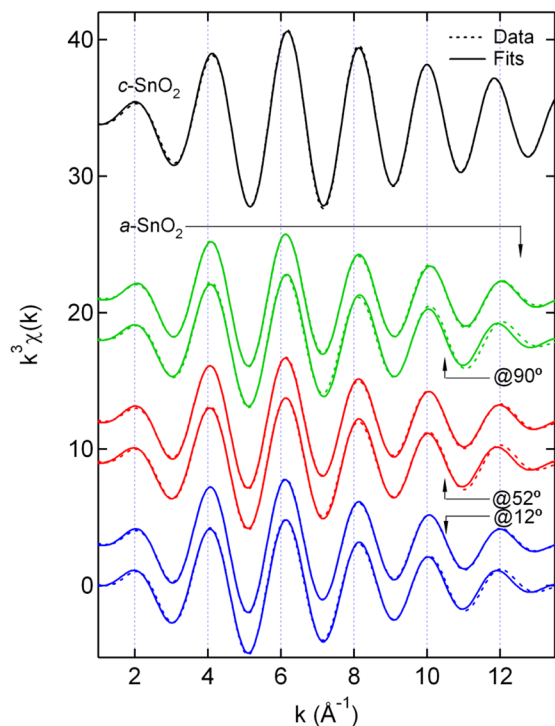


FIG. 4. The fits of the first neighbor EXAFS for $a\text{-SnO}_2$ assuming a single Sn-O shell and two Sn-O shells, respectively. The better fits are due to two-shell fittings (the upper curve for each angle). The result for $c\text{-SnO}_2$ is also shown for comparison for which only a single Sn-O bond distance is assumed. Note that a beating is formed around 9 \AA^{-1} (for a better view, see Fig. S2 in supplementary material⁷).

Table I shows the fitting results obtained using the data up to $k_{max} = 11.6 \text{ \AA}^{-1}$. Note that N_1 is associated with the short Sn-O bonds while N_2 with the long ones. It is seen that the details of N_1 and N_2 are indifferent in terms of the fitting quality as measured by R-factor. However, the results with larger ΔR are favored by the fact that it results in a beat positioned ($\sim\pi/2\Delta R$) closer to the one seen in the backscattering amplitudes (see Fig. S4 in Ref. 7). Moreover, for $\theta = 90^\circ$, the σ^2 value for two short Sn-O bonds is unreasonably smaller (0.0008 \AA^2) than the one (0.0073 \AA^2) for four long Sn-O bonds. Therefore, it is likely that in $a\text{-SnO}_2$ the $[\text{SnO}_6]$ unit is made of, say, four short Sn-O bonds and two long Sn-O bonds. On average, $R_{Sn-O} = 2.029 \text{ \AA}$ and $R_{Sn-O} = 2.130 \text{ \AA}$. Contrary to $c\text{-SnO}_2$, whose ΔR is only 0.015 \AA , the octahedral $[\text{SnO}_6]$ in $a\text{-SnO}_2$ undergoes a distortion similar to that found in transition metal oxides (the Jahn-Teller effect).

The differences in the second shell interaction, which is dominated by the Sn-Sn interaction, are apparent, as shown in Fig. 2(b). The differences are also shown in k space in Fig. S6 in Ref. 7. Simple analytical analyses suggest that the differences are largely due to the Debye-Waller effect. The σ^2 value of $52^\circ\text{-}\chi(k)$ is 10% and 20% larger than those of $12^\circ\text{-}\chi(k)$ and $90^\circ\text{-}\chi(k)$, respectively, indicating that the Sn-Sn interaction is more ordered along the film surface and thickness directions, which may be intimately related with the structures of the first coordination shells. Detailed fittings were also carried out in an R range from 1 to 4 \AA , which produce essentially the same conclusion (see Fig. S7 in Ref. 7) and from which it is estimated that the O-Sn-O bond angle may vary in an angular range $\pm 5^\circ$ around the one ($\sim 102^\circ$) found in $c\text{-SnO}_2$.

For an octahedral symmetry, $N(\phi) (= \sum_i^N 3 \cos^2 \phi_i) = N$. The fact that S_0^2 (or N) of $a\text{-SnO}_2$ is about 3% smaller near the magic angle than that of $c\text{-SnO}_2$ is likely indicative of the oxygen vacancies in $a\text{-SnO}_2$. Moreover, the θ -dependence of the coordination number can only be accounted for by a preferential distribution of the oxygen vacancies along the film surface direction along which a smaller projected $N(\phi)$ is measured. Approximating the density ρ of the $a\text{-SnO}_2$ film with that of bulk SnO_2 ($= 6.95 \text{ g/cm}^3$) the number of oxygen vacancies would be 10^{21} cm^{-3} . The oxygen vacancies may play an important role in the electrical conductivity of the $a\text{-SnO}_2$ film; it is speculated that their preferential distribution may contribute as well. The underlying cause of such an ordering of oxygen vacancies is elaborated in Ref. 7, to which large impact (i.e., momentum

TABLE I. Two Sn-O distance fitting results of the first coordination shell.^a

$a\text{-SnO}_2$	ΔR (\AA)	σ^2 (\AA^2)	R-factor	ΔE (eV)
At 12°	$N_1/N_2 = 2/4$	0.086 / 0.0018/0.0066	0.0016	6.3
	$N_1/N_2 = 4/2$	0.122 / 0.0028/0.0035	0.0015	6.2
At 52°	$N_1/N_2 = 2/4$	0.055 / 0.0019/0.0095	0.0023	6.0
	$N_1/N_2 = 4/2$	0.106 / 0.0035/0.0064	0.0024	6.0
At 90°	$N_1/N_2 = 2/4$	0.086 / 0.0008/0.0073	0.0021	7.4
	$N_1/N_2 = 4/2$	0.134 / 0.0019/0.0030	0.0012	7.4

^aCorresponding S_0^2 values are shown in Fig. 3 for $k_{max} = 11.6 \text{ \AA}^{-1}$. N_1 is associated with the short bonds while N_2 with the long ones.

transfer) during the pulsed laser deposition is attributed. It is suggested that the film is compressively strained which will lower the local structural symmetry. One possible consequence of this uniaxial strain is discussed with reference to the *c*-SnO₂. The impact effect should decrease with increasing deposition pO₂ pressure.

In summary, polarization-dependent X-ray absorption measurements at the Sn K edge reveal the existence of anisotropy in the local structure of a conducting *a*-SnO₂ film prepared by pulsed laser deposition. The differences are readily seen for the second neighbors, where the Sn-Sn interaction dominates. These differences can be accounted for largely by a Debye-Waller effect. The Sn-Sn interaction is ordered most along the film surface direction. Instead of a single Gaussian distribution found in *c*-SnO₂, the distribution of the Sn-O bond distances within the first shell appears to be bimodal, and their separation is slightly better defined along the film surface and thickness directions, indicating the presence of anisotropy in the first coordination as well. The smaller coordination number found in *a*-SnO₂ suggests the existence of oxygen vacancies, which distribute preferentially along the film surface direction.

Film growth, electrical characterization, and X-ray absorption measurements were supported by the NSF Materials Research Science and Engineering Center at Northwestern under Grant No. DMR-1121262. Optical

characterization and structural analysis were supported by the ANSER Center, an Energy Frontier Research Center funded by the U.S. Department of Energy, Office of Basic Energy Sciences, under Award No. DE-SC0001059. X-ray absorption measurements were conducted at the DND-CAT at the Advanced Photon Source (APS). DND-CAT was supported by E.I. DuPont de Nemours & Co., The Dow Chemical Company, and the State of Illinois. Use of the APS was supported by the U.S. Department of Energy, Office of Science, Office of Basic Energy Sciences, under Contract No. DE-AC02-06CH11357.

¹E. Fortunato, D. Ginley, H. Hosono, and D. C. Paine, *MRS Bull.* **32**, 242 (2007).

²D. C. Paine, B. Yaglioglu, Z. Beiley, and S. Lee, *Thin Solid Films* **516**, 5894 (2008).

³J. S. Lannin, *Phys. Today* **41**(7), 28 (1988).

⁴W. H. Zachariasen, *J. Am. Chem. Soc.* **54**, 3841 (1932).

⁵J. C. Phillips, *Phys. Today* **60**(11), 10 (2007).

⁶J. Tafto, G. Rajeswaran, and P. E. Vanier, *J. Appl. Phys.* **60**, 602 (1986).

⁷See supplementary material at <http://dx.doi.org/10.1063/1.4815984> for more details.

⁸W. H. Baur and A. A. Khan, *Acta Crystallogr., Sect. B* **27**, 2133 (1971).

⁹R. F. Pettifer, C. Brouder, M. Benfatto, C. R. Natoli, C. Hermes, and M. F. R. Lopez, *Phys. Rev. B* **42**, 37 (1990).

¹⁰J. J. Rehr and R. C. Albers, *Rev. Mod. Phys.* **72**, 621 (2000).

¹¹B. Ravel and M. Newville, *J. Synchrotron Radiat.* **12**, 537 (2005).

¹²G. Martens, P. Rabe, N. Schwentner, and A. Werner, *Phys. Rev. Lett.* **39**, 1411 (1977).